

B. MOMENI
A. ADIBI[✉]

Optimization of photonic crystal demultiplexers based on the superprism effect

School of Electrical and Computer Engineering, Georgia Institute of Technology, Atlanta, GA 30332, USA

Received: 26 March 2003/Revised version: 27 June 2003
Published online: 14 October 2003 • © Springer-Verlag 2003

ABSTRACT We present a general method for the optimization of two-dimensional photonic crystal demultiplexers based on the superprism effect. We define and use two figures of merit, representing the compactness and ease of realization of the structure. Based on these criteria, the effects of various design parameters on the performance of these demultiplexers are discussed, and various structures are compared. Our results suggest that triangular lattice photonic crystals with a boundary along the ΓM direction and TE polarization are the best candidates for designing superprism-based demultiplexers.

PACS 42.79.-e; 42.70.Qs

1 Introduction

Photonic crystals (PCs) [1, 2] have inspired a lot of interest recently due to their potential for controlling the propagation of light. In most applications proposed to date, photonic crystals have been used primarily because of their photonic band gap, in which the propagation of light is prohibited. Some examples of such applications are the reduction of spontaneous emission [1], the control of the flow of light in photonic crystal waveguides [3], and cavity-based applications [3, 4]. However, there are other applications based on the propagation of light inside photonic crystals. These applications mainly rely on the anomalous dispersion behavior of photonic crystals. Lin et al. were the first to propose the use of photonic crystals in the propagating regime for wavelength separation in a prism-like structure [5]. Later, Kosaka et al. suggested another potential use based on the anomalous dispersion of photonic crystals [6], proposing a highly sensitive phenomenon, named the superprism

effect, for wavelength-demultiplexing applications [7]. The phenomenon has been well explained based on the group velocity direction and its relation to the band structure [8, 9]. The implementation of wavelength separation in a planar photonic crystal structure has been demonstrated, with good agreement with theory being obtained [10]. Also, some implementation issues and basic limitations and considerations of superprism-based demultiplexers have been addressed and discussed [11, 12].

For the efficient realization of practical superprism-based demultiplexers, it is necessary to define proper measures of the performance of these structures and to study the effect of various design parameters on such performance measures. In this letter, we propose two performance measures and use them to find the optimum design parameters for effective PC demultiplexing using the superprism effect. We focus our discussion on two-dimensional planar structures due to their relatively easy fabrication and their consistency with integrated optics platforms, which make

them the most feasible choice for the actual realization of photonic crystal circuits. The best design for each particular structure is then found by direct optimization. Having this optimum design, the actual specifications of the demultiplexer (for example, channel spacing, angle of incidence, and divergence of input beam) can be found for the desired demultiplexing properties.

2 Analysis

The basic configuration for the PC wavelength demultiplexer that is studied throughout this paper is shown in Fig. 1. The same configuration will be used to study and compare the performance of different demultiplexers using several PC lattices and geometries. The PC is illuminated by a collimated input beam from a homogeneous medium (for example, air) with refractive index n_1 . Due to the anomalous dispersion property of the PC, different wavelengths are spatially separated at the output (wavelength demultiplexing). Although we primarily consider a photonic crystal of air holes in Si, our approach can be used for photonic crystals of dielectric rods in air as well.

The parameters that can be used in designing such PC demultiplexers are the divergence angle of the input beam, the angular separation between adjacent wavelength channels inside the PC, and the angle of incidence of the input beam. A simple measure to compare the performance of different PC demultiplexers is the compactness of the structure, which is directly related to the area of the structure for demultiplexing a given number of channels. In this context, the design parameters are to be found so as

✉ Fax: +1-404/894-4641, E-mail: adibi@ee.gatech.edu

to realize wavelength demultiplexing of a certain number of channels with the smallest possible area of the structure.

We assume the incident beam (which is composed of multiple frequency channels) to be spatially Gaussian, which is a good approximation for most practical cases. To properly analyze the structure in Fig. 1, we need to model and study the propagation of optical beams inside the PC region. If the divergence of the incident beam is small, the range of excited Bloch wave vectors inside the PC region at each incident frequency is limited. Thus, we can approximate the shape of the band structure within the range of excited Bloch wave vectors by a quadratic curve. In this way, at each particular frequency, the corresponding constant frequency contour of the PC band structure in k -space is locally approximated by a quadratic approximation that is similar to the behavior of the contours in a homogeneous isotropic medium. Since the effective index of refraction that defines the divergence of the beam is given by the curvature of the band structure [13], the effective index for the PC region can be found from this curvature (similar to an isotropic bulk region); that is,

$$\begin{aligned} n_e &= \frac{1}{k_0 \left(\partial^2 k_\eta / \partial k_\xi^2 \right)} \\ &= \frac{n_1 \cos \alpha}{(\partial \theta_g / \partial \alpha) \cos \theta_g} \\ &= \frac{1}{\cos \theta_g} \frac{\partial}{\partial \theta_g} \left(\frac{k_t}{k_0} \right), \end{aligned} \quad (1)$$

where k_η and k_ξ are the wave-vector components parallel and normal, respectively, to the direction of propagation of the beam inside the PC. Furthermore, n_1 is the refractive index of the incidence region, α is the angle of incidence, θ_g is the angle of the group velocity inside the PC with respect to the normal to the interface, k_t is the magnitude of the tangential component (with respect to the interface of the PC region) of the wave vector, and k_0 is the free-space wave number. Note that the electromagnetic boundary conditions at the interface of the two regions in Fig. 1 require the continuity of k_t across the interface. Different parameters in (1) are shown graphically in Fig. 1. The complete derivation of (1) can be found in [13].

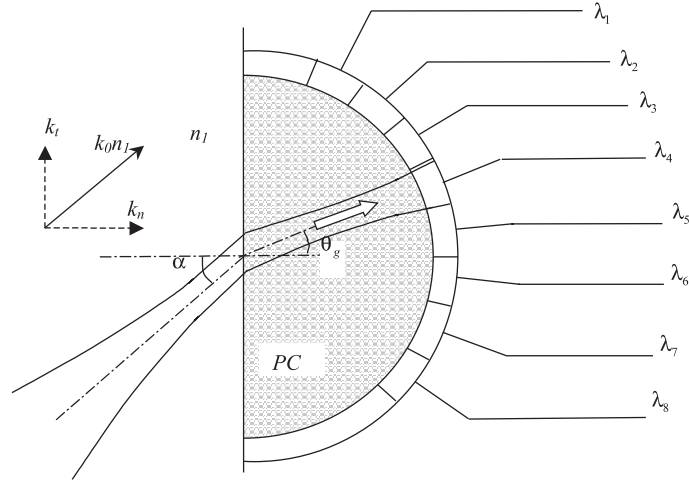


FIGURE 1 Geometrical structure used for demultiplexing

Note that the effective index n_e depends on the wavelength and incident angle. Using this model we can analyze the propagation of light beams inside the PC region using conventional techniques to avoid long numerical simulations. For example, an incident Gaussian beam will propagate as a Gaussian beam inside the PC when this approximation is valid. Thus, we can use the known formulas for the beamwidth and divergence angle of an optical beam to calculate the properties of the beam inside the PC. The accuracy of this approximation depends on the deviation of

the actual PC band structure from the quadratic approximation over the spatial bandwidth (or the range of excited Bloch wave vectors) of the optical beam inside the PC. The actual condition on the spatial bandwidth depends on the PC band structure and the center wavelength of operation.

The field profiles at different propagation lengths inside the PC for an incident Gaussian beam at normal incidence are shown in Fig. 2. To calculate these curves, the incident beam profile at each frequency is expanded over plane-wave components. For each inci-

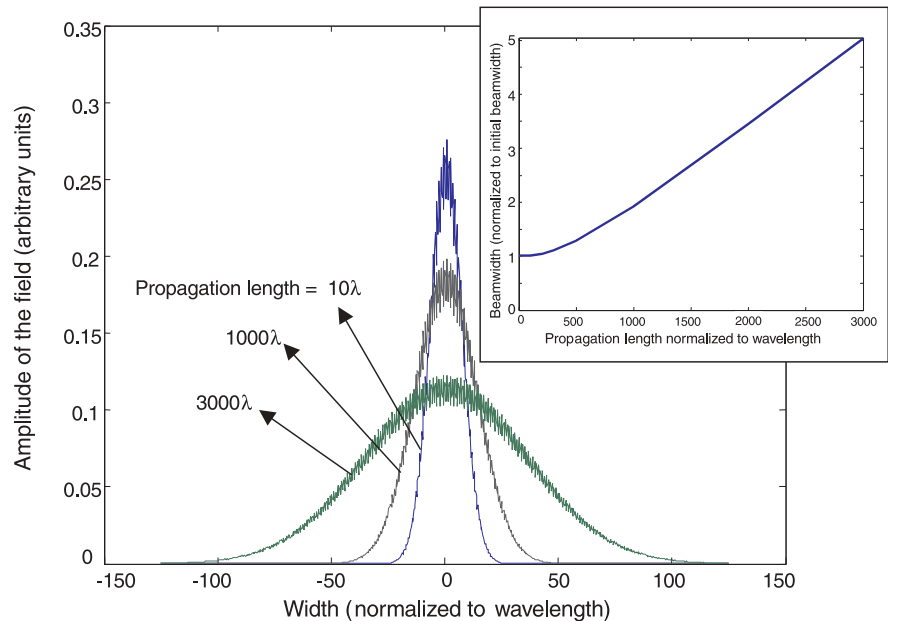


FIGURE 2 Field patterns of the beam inside the photonic crystal at different propagation lengths. The photonic crystal is a square lattice of air holes in Si, with the ratio of the radii of the holes to the lattice constant equal to 0.40, and the lattice constant equal to 0.24λ . The incident beam is Gaussian with TE polarization at normal incidence

dent plane wave, the total field in the incident region is expanded over reflected and evanescent plane waves, and the field inside the PC region is expanded over PC modes. The modes in the PC region are expressed by their plane-wave expansion representations, and using the mode-matching method, the amplitudes of all components in the mode expansions in both the incident and PC regions are found. By superposition of all incident plane-wave components after propagation inside the PC, the field profiles inside the PC region at different propagation lengths are calculated [13]. The photonic crystal in this case is a square lattice of air holes in Si ($\epsilon_r = 11.4$), and the radius of the holes is $r = 0.40a$, where a is the lattice constant. The incident beam comes from air with TE polarization (electric field normal to the plane of periodicity of the PC), and at a wavelength $\lambda = a/0.24$. The TE photonic band gap for this structure is $0.222 < (a/\lambda) < 0.226$. The fluctuations in the beam profiles are due to the spatial variations of the permittivity in the PC region. The overall pattern (or envelope) of the beam is Gaussian everywhere and is not affected by these small variations.

To find the optimum design for each structure, we first calculate the two-dimensional band structure of the PC. Then, we find all the modes of the PC excited by each plane wave incident at an angle α and with a normalized frequency of $\omega_n = \omega a/2\pi c$ (c is the velocity of light in a vacuum), and calculate $\theta_g(\omega_n, \alpha)$, the angle of the group velocity corresponding to these excited modes of the PC. By changing α and ω_n and repeating the calculations, we find the function $\theta_g(\omega_n, \alpha)$ for all incident angles and frequencies of interest.

While a rapid variation of θ_g with ω_n is desired for demultiplexing purposes, this behavior usually appears along with a high sensitivity of θ_g to the angle of incidence α . In fact, the main limitation that restricts the separation of wavelengths inside a PC structure is the cross-talk caused by the divergence of the input beam. In other words, for angles slightly different from α , yet inside the divergence angle of the input beam (i.e., in the range $\Delta\alpha$ around α), the high angular sensitivity of the structure causes the signal for one channel to interfere with those of its neighboring

channels. To avoid mixing of adjacent channels, a very small divergence of the input beam is needed, which makes the structure relatively large [12].

After finding the function $\theta_g(\omega_n, \alpha)$, we must choose the range of angles to be used for the separation of different channels in space. It might seem reasonable to use the entire angular range of θ_g (from minimum θ_g to maximum θ_g) for demultiplexing. In [12], the whole range of θ_g at a specific angle of incidence was used for demultiplexing. Although the whole range of available channels was used in this way, there are regions of θ_g with very high sensitivity to the angle of incidence. This large sensitivity results in a highly divergent beam inside the PC. Thus, the size of the structure is increased (to avoid cross-talk) without having a significant effect on the demultiplexing capability. Here, we exclude the regions of the band structure with very high sensitivities to the angle of incidence by limiting our design to the regions with $\partial\theta_g/\partial\alpha < \beta$. We call β the angular sensitivity threshold. Applying this restriction for each angle of incidence α and angular sensitivity threshold β , we can find the

total available range of variations of the group velocity angle, $\theta_T(\alpha, \beta)$. It should be noted that in defining θ_T directly as a function of α and β , a single value of α is used for the entire incident signal, and the divergence of the input signal ($\Delta\alpha$) is neglected. If the input beam has a large divergence, the angular selectivity of the structure comes into the picture and a degradation factor should be considered. In our case, however, the number of channels is large and, as a result, the divergence of the beam is relatively small. Therefore, expressing $\theta_T(\alpha, \beta, \Delta\alpha) \approx \theta_T(\alpha, \beta)$ is a valid assumption.

Figure 3a shows the band structure for a 2D square lattice of air holes (with radius $r = 0.35a$) in the form of constant frequency contours calculated by a plane-wave expansion [14]. Only the second TE (electric field normal to the plane of periodicity of the PC) band, which is of interest in designing demultiplexers, is shown here. We have also shown in Fig. 3a the group velocity contours (loci of points in the 2D k -space with a constant angle of the group velocity, θ_g). Only group velocity contours with a 5° separation of θ_g

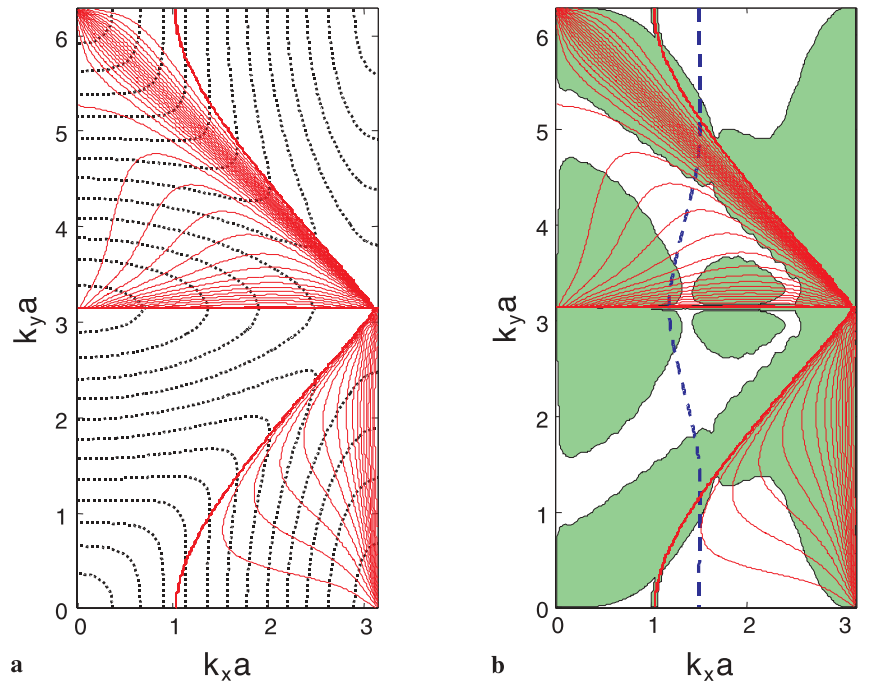


FIGURE 3 **a** Constant frequency contours (*dotted lines*) for the second TE band in the square lattice of air holes ($r/a = 0.35$) in Si, and group velocity contours (*solid lines*, loci of the points in 2D k -space with a constant angle of the group velocity inside the PC) of the modes that can be excited by a plane wave incident from air with the interface along the x -direction. To avoid confusion, we have only shown constant angle contours with a 5° separation between adjacent contours. **b** Same band structure as in **(a)**, with *shaded regions* representing the corresponding regions that should be excluded with a $\beta < 0.25$ criterion. The *dashed line* corresponds to an angle of incidence of $\alpha = 62^\circ$ from air

are shown. In Fig. 3b, we have shaded some areas, which represent the regions with high sensitivity of θ_g to α (i.e., $\beta > 0.25$). In designing a PC demultiplexer, we exclude these regions to avoid very large beams inside the PC. In these simulations we have used 961 plane-wave components and we expect the computation error due to the finite number of plane waves to be less than 1% [15]. In Fig. 3b, we can see that the range of the band structure that is actually used for demultiplexing purposes in an appropriately designed device coincides with the region in which the band structure of the PC is well-behaved. In these regions the quadratic approximation that was assumed in deriving (1) is valid for practical optical beams. In fact, in these regions the allowed divergence of the input beam for a practical demultiplexer is so small that the optical beams inside the PC are narrowband enough to pass the criterion for (1).

3 Figures of merit

For demultiplexing N_c channels, we assume the angular separation between successive channels to be $\Delta = \theta_T/N_c$. From the effective index model given in (1), the divergence angle of each channel, δ , can be written as

$$\delta = \frac{2\lambda}{\pi n_e w_0}, \quad (2)$$

with $2w_0$ being the minimum waist of the beam. To have channel separation, we may assume

$$\Delta = \delta. \quad (3)$$

Our simulations show that for adjacent channels to be spatially separated, the propagation length should be at

least $R = 2z_0$, where $z_0 = 4\lambda/(\pi n_e \delta^2)$ is the Rayleigh range for Gaussian beam propagation inside the PC. Putting these values together, the size of the structure can be written as

$$A = \frac{\theta_T}{2} R^2 \cong \frac{\theta_T}{2} \left(\frac{8\lambda}{\pi n_e \delta^2} \right)^2. \quad (4)$$

Therefore, from (1), (3), and (4), the normalized size of the structure is found to be

$$\begin{aligned} A_N &= \frac{A}{\lambda^2} \cong \frac{32}{n_1^2 \pi^2} \left(\frac{\beta^2}{\theta_T^3 \cos^2 \alpha} \right) N_c^4 \\ &= \frac{N_c^4}{C(\alpha, \beta)}, \end{aligned} \quad (5)$$

where the compactness factor, $C(\alpha, \beta)$, is defined as

$$C(\alpha, \beta) = \frac{n_1^2 \pi^2 \theta_T^3(\alpha, \beta) \cos^2 \alpha}{32 \beta^2}. \quad (6)$$

In these calculations we have considered the approximation for the worst case by neglecting the effect of $\cos \theta_g$ factor.

It can be observed that for specific design values for α and β , the size of the structure increases as the fourth power of the number of channels. This encourages us to use a cascading scheme when high wavelength resolution (or a large number of channels) is needed. Assuming the cascaded superprism stages to be similar in size, with each separating N_{cas} channels, the beamwidth is reduced by a factor of N_c/N_{cas} , and the size of the structure is on the order of

$$A_N^{\text{Cascaded}} \approx C^{-1} N_c N_{\text{cas}}^3 \log_{N_{\text{cas}}}(N_c), \quad (7)$$

which can be much less than the original single-stage structure. As an example, for $N_c = 64$ and $N_{\text{cas}} = 4$, we have $A_N^{\text{Single-stage}}/A_N^{\text{Cascaded}} \sim 10^2-10^3$.

The price we pay in cascading the structures is added complexity and extra loss in coupling successive stages.

Another issue that affects how easy the device can be realized is the required divergence of the input beam. Using simple calculations at the interface, the divergence angle of the input beam, $\Delta\alpha$, is found to be

$$\Delta\alpha = \frac{\delta}{\beta} = \left(\frac{\theta_T(\alpha, \beta)}{\beta} \right) \frac{1}{N_c}, \quad (8)$$

in which the input divergence is inversely proportional to the number of channels. Based on this result, we define the ‘‘ease of realization’’ parameter, $E(\alpha, \beta)$, by

$$E(\alpha, \beta) = \frac{\theta_T(\alpha, \beta) \cos \alpha}{n_1 \beta}. \quad (9)$$

4 Optimization results

Depending on the specific goal for the design, an appropriate combination of $C(\alpha, \beta)$ and $E(\alpha, \beta)$ can be used for optimization. Here, we choose our goal function as $G(\alpha, \beta) = C(\alpha, \beta)E(\alpha, \beta)$, which is to be maximized. We find the values of the goal function over the entire (α, β) plane and use a direct search method to find its maximum. The results for different structures are summarized in Table 1. It can be seen that the proper choice of the photonic crystal is very important for the performance of the resulting device. The results shown in Table 1 suggest that the best performance among the structures under study is obtained by using a triangular lattice in the ΓM direction with TE polarization. Figure 4 shows the variation of the goal function with the radii of the air holes for

| Lattice, direction | r/a | Pol. | β_G | α_G (°) | θ_{TG} (°) | C | E | G |
|--------------------------------|-------|------|-----------|----------------|-------------------|-------|-------|-------|
| Triangular Lattice, ΓM | 0.15 | TE | 0.07 | 18 | 13.0 | 0.644 | 3.04 | 1.95 |
| Triangular Lattice, ΓM | 0.20 | TE | 0.023 | 24 | 6.88 | 0.844 | 4.77 | 4.03 |
| Triangular Lattice, ΓM | 0.25 | TE | 0.054 | 30 | 10.8 | 0.538 | 3.05 | 1.64 |
| Triangular Lattice, ΓM | 0.30 | TE | 0.026 | 36 | 5.63 | 0.273 | 3.00 | 0.820 |
| Triangular Lattice, ΓM | 0.35 | TE | 0.060 | 42 | 6.60 | 0.069 | 1.39 | 0.095 |
| Triangular Lattice, ΓM | 0.40 | TE | 0.14 | 46 | 7.98 | 0.020 | 0.674 | 0.013 |
| Triangular Lattice, ΓM | 0.15 | TM | 0.51 | 12 | 23.1 | 0.074 | 0.772 | 0.057 |
| Triangular Lattice, ΓK | 0.35 | TE | 2.1 | 40 | 110 | 0.289 | 0.700 | 0.202 |
| Triangular Lattice, ΓK | 0.25 | TM | 4.9 | 16 | 100 | 0.064 | 0.346 | 0.022 |
| Square Lattice, ΓM | 0.35 | TE | 0.25 | 62 | 15.1 | 0.020 | 0.490 | 0.010 |
| Square Lattice, ΓM | 0.35 | TM | 3.2 | 58 | 124 | 0.086 | 0.359 | 0.031 |

TABLE 1 Comparison of different PC structures for wavelength demultiplexing (optimization for $G = CE$)

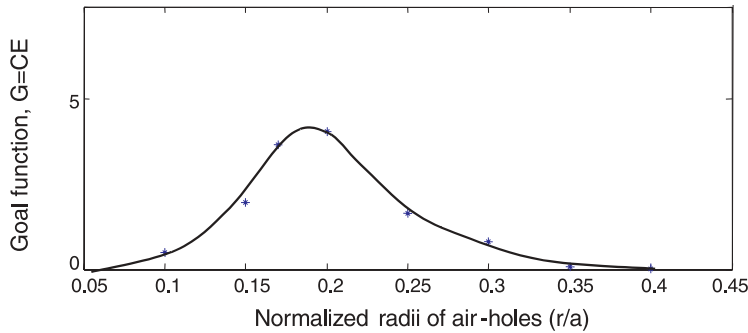


FIGURE 4 Goal function with respect to the radii of the air holes in a triangular lattice of air holes in Si ($\epsilon_r = 11.4$) with the ΓM direction parallel to the interface with air. The polarization of the incident beam is TE. The *solid curve* shows the interpolation of the actual data points

TE modes in the ΓM direction of a triangular lattice. It is clear from Fig. 4 that there is an optimum value of r/a for which the goal function is a maximum. This demonstrates the importance of an appropriate choice of the size of the radii of the holes. Note that the optimum structure for superprism demultiplexing is different from the structure with the largest band gap. (In this case, the maximum band gap occurs at $r/a = 0.40$ with TM polarization, and at $r/a = 0.48$ with TE polarization.)

After optimizing each PC structure (lattice type, direction), the best design values for α_G , β_G , and $\theta_T(\alpha_G, \beta_G)$ are known. Using these values, for any desired number of channels, several quantities can be determined. First, from $\Delta = \theta_T/N_c$, the angular separation between the channels inside the PC can be found. Second, using $\Delta = \delta$ and $R = 8\lambda/(\pi n_1 \delta^2 \cos \alpha)$, the size of the structure is obtained. Finally, from (8), the required divergence angle of the input beam can be calculated. These values define the complete design for demultiplexing N_c channels in the optimum way.

For a complete design, we have to check the validity of the effective index model used for this optimization. Now that the incident beam, the angle of incidence, and the photonic crystal structure is known, we can easily find the range of PC modes excited by the incident beam, and the corresponding curve. For the given propagation length, the contribution of higher order terms for this range of photonic crystal modes has to be negligible for our effective index model to be valid (this validity is equivalent to the beam shape being well-behaved). Having all the parameters for a design, this issue can be easily checked.

Up to this point we have not imposed any condition on the frequencies of the channels. Our primary design criteria was an equal angular separation ($\Delta = \theta_T/N_c$) between adjacent channels. The frequencies of different channels in the optimum structure are not equally spaced. This type of demultiplexer is perfect for spectroscopic applications for which the goal is to separate and measure the optical signal at different wavelengths. If an implementation for a conventional WDM demultiplexer with a particular frequency separation between channels is required, we may use the same designs as above. However, because of nonlinear variations of the angle of the channels with the frequency of the channels, we may need to readjust the angles of the channels to have a particular (equal) frequency separation between adjacent channels. In this process, our structure is used to demultiplex fewer channels than optimally possible to generate a uniform spacing between the channel frequencies. Thus, the number of available channels may be degraded in this process, but the basic ideas still can be used.

Note that the effective index model described in this paper is useful for the analysis of the propagation of light inside the PC structures (as long as the quadratic approximation of a constant frequency contour is valid), but it cannot be used for the calculation of the reflection and transmission coefficients at the boundary of the PC and the incident medium (for example, air). The reason is that the effective index model was developed based on the propagation behavior of the propagating modes in the PC region. On the other hand, in applying boundary conditions to find the transmission and reflection coefficients

at a boundary, both propagating modes and evanescent modes in the near field must be considered.

Finally, it must be noted that the results of this paper were calculated using two-dimensional (2D) simulations. For practical structures, the finite thickness of the structure must also be taken into account. This primarily modifies the band structure of the PC for in-plane propagation. However, the optimization method presented in this paper is general and can be applied to the modified band structures. The 2D optimized results can be used as the initial step for a more accurate 3D optimization. Furthermore, the method can be easily applied to any other PC structures made in substrates other than Si.

5 Conclusions

In conclusion, we have presented a general method for the optimization of 2D photonic crystal demultiplexers that rely on the superprism effect. We chose the area of the structure and the divergence angle of the input beam to be the practical measures for the quality of the structure. We defined two figures of merit for the ease of realization (E) and compactness of the structure (C), and optimized several structures to obtain the best design for the desired number of channels. We showed that the ease-of-realization decreases linearly with an increasing number of channels, while the area of the structure increases with the fourth power of the number of channels in a basic superprism-based photonic-crystal demultiplexer. These relations encouraged us to use a cascading scheme for demultiplexing a large number of channels instead of having a single superprism stage. Our results suggest that a triangular-lattice photonic crystal in the ΓM direction can provide the best demultiplexing performance.

ACKNOWLEDGEMENTS This work was supported by the Air Force Office of Scientific Research (G. Pomrenke) and by the David and Lucile Packard Foundation.

REFERENCES

- 1 E. Yablonovitch: Phys. Rev. Lett. **58**, 2059 (1987)
- 2 S. John: Phys. Rev. Lett. **58**, 2486 (1987)
- 3 J. Joannopoulos, R. Meade, J. Winn: *Photonic Crystals: Molding the Flow of Light* (Princeton University Press, Princeton 1995)

- 4 C. Weisbuch, H. Benisty, R. Houdre: *J. Lumin.* **85**, 271 (2000)
- 5 S.Y. Lin, V.M. Hietala, L. Wang, E.D. Jones: *Opt. Lett.* **21**, 1771 (1996)
- 6 H. Kosaka, T. Kawashima, A. Tomita, M. Notomi, T. Tamamura, T. Sato, S. Kawakami: *Phys. Rev. B* **58**, R10096 (1998)
- 7 H. Kosaka, T. Kawashima, A. Tomita, M. Notomi, T. Tamamura, T. Sato, S. Kawakami: *J. Lightwave Technol.* **17**, 2032 (1999)
- 8 M. Notomi: *Phys. Rev. B* **62**, 10696 (2000)
- 9 B. Gralak, S. Enoch, G. Tayeb: *J. Opt. Soc. Am. A* **17**, 1012 (2000)
- 10 L. Wu, M. Mazilu, T. Karle, T.F. Krauss: *IEEE J. Quantum Electron.* **QE-38**, 915 (2002)
- 11 T. Baba, D. Ohsaki: *Jpn. J. Appl. Phys.* **40**, 5920 (2001)
- 12 T. Baba, T. Matsumoto: *Appl. Phys. Lett.* **81**, 2325 (2002)
- 13 B. Momeni, A. Adibi: *IEEE J. Lightwave Technol.* (2003); submitted
- 14 R.D. Meade, A.M. Rappe, K.D. Bromme, J.D. Joannopoulos, O.L. Alerhand: *Phys. Rev. B* **48**, 8434 (1993)
- 15 L. Shen, S. He: *J. Opt. Soc. Am. A* **19**, 1021 (2002)